Composites Part B 307 (2025) 112927

Contents lists available at ScienceDirect

Composites Part B

journal homepage: www.elsevier.com/locate/compositesb

Characterisation of thermoplastic sandwich panels manufactured by continuous ultrasonic welding of skins to the core

Amal Alliyankal Vijayakumar [a,*], Muhammad Zahid [b], Stefano G. Corvaglia [c], Francesco Montagna [a], Francesca Lionetto [a], Alfonso Maffezzoli [a]

[a] Department of Engineering for Innovation, University of Salento, Via per Monteroni, 73100, Lecce, Italy
[b] Quantum Technologies, Optronics & Material Laboratories, Innovation Labs, Leonardo S.p.A., St. Prov. Grottaglie-Monteiasi 83, 74023, Grottaglie, Italy
[c] Engineering – Technology Research & Innovation, Aerostructure Division, Leonardo S.p.A., St. Prov. Grottaglie-Monteiasi 83, 74023, Grottaglie, Italy

ARTICLE INFO

Handling Editor: Dr Uday Vaidya

Keywords:
Ultrasonic welding
Mode I
Thermoplastic sandwich structures
Foam core
E-glass/PP skins

ABSTRACT

Continuous ultrasonic welding is an emerging, fast, and energy-efficient technique for joining thermoplastic composite structures. This research emphasises its potential as an innovative approach for achieving continuous skin/core bonding in manufacturing mono-polymer thermoplastic sandwich structures. Therefore, this study aims to develop a continuous ultrasonic skin/core welding setup equipped with a horn and a compaction roller. A single cantilever beam (SCB) fracture toughness test was conducted on sandwich panels, manufactured using commingled E-glass/polypropylene (PP) skins and a PP foam core, to assess the quality of skin/core welding under different welding conditions. Mode I fracture toughness was measured at various welding speeds (e.g., 4-, 5- and 6 mm/s) and horn pressures (e.g., 0.17-, 0.28- and 0.39 MPa) using two data reduction methods, accounting for assumptions related to compliant skin specimens. Variations in processing parameters significantly impact heat generation and its distribution at the skin/core interface, thereby affecting the weld quality. Hence, careful optimisation of processing conditions ensures a sustainable manufacturing route for sandwich panels, enabling efficient assembly, rapid processing times, and the manufacturing of thermoplastic sandwich structures.

1. Introduction

Sandwich structures are made of two stiff and thin skins, supporting compressive and tensile stresses under bending loads, bonded to a low-density core to carry shear loads from the transverse loading. This symmetric three-layer system makes the structure an efficient load-carrying component for various critical load-bearing applications [1,2]. The thermoset-based, well-established sandwich panels fail to meet sustainability needs and are associated with intense production costs and time. In contrast, thermoplastic sandwich structures have driven much of the attention nowadays due to their excellent performances, such as lightweight, acoustic, and thermal damping capabilities, recyclability, high specific strength and stiffness, and ease of thermoforming [3,4]. Therefore, they garner significant interest across the marine, aerospace, automotive, rail, and sporting industries.

Structural failure in sandwich structures, including skin/core debonding, core-shear failure, core indentation, skin wrinkling, and shear crimping and buckling of the skin or the core, can arise during in-service use [5]. Among these, skin/core debonding is a significant concern that disrupts the transfer of bending loads, compromising the system's structural integrity [5–7]. Therefore, the skin/core bonding plays a pivotal role in determining the overall structural stability and performance of sandwich structures. Ongoing concerns with adhesive bonding make fusion bonding a promising approach for joining the thermoplastic skin and core materials through molecular interdiffusion [2,3,8]. Manufacturing technologies such as vacuum bagging, double belt lamination, compression moulding, and in-situ foaming (through film foaming and injection moulding) are widely adopted in industrial processes for achieving skin/core fusion bonding, more commonly known as fusion welding [2]. In manufacturing complex shapes and structures, these technologies possess economic and technological drawbacks, requiring complex moulds and multiple interlinked processing steps [9]. The distinctive characteristics of continuous ultrasonic welding (USW) of fibre-reinforced thermoplastic composites (FRTPCs), on the other hand, offer an efficient and effortless solution for fusion welding, especially suited for complex designs and are easily

* Corresponding author.
E-mail address: amal.av@unisalento.it (A. Alliyankal Vijayakumar).

https://doi.org/10.1016/j.compositesb.2025.112927
Received 1 May 2025; Received in revised form 15 August 2025; Accepted 17 August 2025
Available online 19 August 2025

automatized [10–12]. Heat generation at the weld interface under high frequency (20–40 kHz) and low amplitude (20–60 μm) ultrasonic vibration is attributed to either boundary friction arising from surface asperities or viscoelastic heating driven by intermolecular friction. Until now, the application of ultrasonic welding (USW) is an emerging process with some pioneering applications confined to joining FRTPCs and dissimilar materials, such as FRTPCs/metals, particularly within the aeronautic sector [13,14]. However, implementing a continuous USW for fusion bonding at the skin-to-core interface of sandwich panels remains a significant challenge and is largely unexplored. For instance, a static USW method for sandwich panels with poly-lactic acid or polyethylene thermoplastic skins reinforced with flax or glass fibres and an upcycled polyethylene honeycomb core was developed and investigated by Oliveira et al. [15]. The skin/core weld interface of similar materials exhibited weaker interface joints, resulting in lower flexural strength than adhesively bonded sandwich structures. Likely, the carbon fibre-reinforced polyetheretherketone (CF/PEEK) composite honeycomb manufactured using multi-spot ultrasonic welding showed poor joint interfaces [16].

The interface characteristics of ultrasonic welding rely on key parameters, including input energy, horn pressure, vibration amplitude, frequency, and welding speed, that directly influence the quality of the weld and bond strength. Wang et al. [17] and Unnikrishnan et al. [18] conducted a comprehensive review of the USW in FRTPCs, focusing on weldability, weld quality, and underlying mechanisms in heat generation and joint formation. The weld time, horn pressure, and amplitude were noted to be significant factors in determining the weld quality and bond strength. Moreover, Lionetto et al. [19] adopted numerical simulation to study the impact of different welding speeds on heat generation and heat transfer during USW. The findings suggested that higher welding speed exhibits a lower melting temperature, leading to improper melting of the polymer. Similar findings were also proven by Filip et al. [20] during the USW of FRTPCs, such that the weld strength is highly dependent on the changing welding speed for a constant amplitude. Furthermore, ultrasonic weld strength depends on both horn or weld pressure and welding time, with optimal values required for each to achieve maximum joint performance [21].

Characterising the skin/core bonding is essential to achieve a reliable assessment of how the process parameters affect the interface performance. The skin/core bonding strength can be effectively quantified by measuring the strain energy release rate, commonly referred to as fracture toughness. Among various fracture modes, the Mode I fracture toughness is significantly important, as it denotes the material's resistance to opening-mode crack propagation, a dominant failure mode in skin/core debonding scenarios [6]. In the Mode I test, the skin is peeled off from the core under the application of an opening load, enabling direct assessment of adhesion at the interface [6,7]. Nonetheless, in practical applications and experimental studies, other stress states arise at the skin/core interface, all related to skin-core adhesion. Also, other failure modes can evolve, such as cohesive failure within the core, skin delamination, or skin wrinkling, with the weakest mode ultimately governing the overall sandwich failure. Four-point bending or out-of-plane skin pull-out is also often used to characterise the skin-core adhesion. However, Mode I fracture testing is commonly used to study interlaminar adhesion in composites, and it can be considered a fundamental and widely accepted method for comparing interface quality. Therefore, it was also adopted in this case, as widely reported in the literature [6,22], as an extension of the approach adopted for composites. A vast variety of non-standardised testing procedures for Mode I fracture toughness in sandwich structures have been developed and conducted, including arrangements such as Climbing Drum Peel (CDP), Double Cantilever Beam (DCB), Tilted Sandwich Debond (TSD), and Single Cantilever Beam (SCB). The asymmetric loading in DCB and TSD induces Mode II (shear) stress components at the crack tips, restricting dominant Mode I testing [6,23]. The CDP method is often used to assess the quality of skin/core bonding with very compliant skins or even polymer films [24]. However, variations in skin conformity with the drum diameters significantly influence the measured fracture toughness values, limiting the applicability of the CDP method for accurately assessing skin/core interfacial fracture toughness [6]. In contrast, the quasi-static SCB testing arrangement, utilising either a long flexible loading rod or a rigid base with roller support, is regarded as a more reliable approach for determining dominant Mode I fracture toughness in sandwich panels [6]. The rotation of the long loading rod or the horizontal movement of the roller base avoids the shear or Mode II component, providing a symmetric or vertical loading at the crack tip. The SCB arrangement with a roller base is ideal for analysing Mode I in stiff skin specimens. This setup effectively measures dominant Mode I fracture toughness for parametric comparisons in thick-skin sandwich structures [22].

This study aims to investigate the skin/core weldability by developing a custom-made ultrasonic welding setup enabling continuous welding of the commingled E-glass/polypropylene (PP) skin with the closed-cell PP foam core. The effect of processing parameters, such as welding speed and horn pressure, on the skin/core welding has been examined by calculating Mode I fracture toughness using an SCB arrangement with a roller base configuration.

2. Experimental methods

2.1. Materials

The used closed-cell foam core with a density of 90 kg/m^3 and a nominal thickness of 27 mm was manufactured by REDSTAMP, Italy. The skins were produced using two plies made of commingled E-glass/PP fabrics, with 745 g/m^2 areal density, supplied by Saint-Gobin Vortex, France, under the commercial name Twintex®. An isothermal compression moulding process using a hydraulic press, Campana P7-91, Italy, was adopted to consolidate the commingled fabric. The skins were consolidated for 40 min at 180 °C under a pressure of 2 MPa. A 150 μm polyimide film (Kapton) was placed on a 270 × 270 × 10 mm^3 aluminium mould to guarantee easy removal of the 1.2 mm thick skin (h_{skin} in Fig. 1). The skins and foam core used for USW were cut to dimensions of 270 mm in length and 40 mm in width using a handsaw. After cutting, the edges were polished using sandpaper to remove any sharp edges or burrs. The skin and core surfaces were then cleaned with acetone to eliminate surface contaminants.

2.2. Skin/core ultrasonic welding setup

The skin/core welding process using 20 kHz ultrasonic welding equipment is depicted in Fig. 1. The USW system comprises a thermoplastic welder (Sonic Italia srl, Italy) capable of producing a peak power of 2 kW and an amplitude of 42 μm. The thermoplastic welder was configured to produce intense mechanical vibrations to a circular 40 mm diameter K100 steel horn, operating at 15 % of maximum power (0.3 kW) and 50 % of maximum amplitude (21 μm). The generated ultrasonic vibrations are responsible for the relative molecular displacements and surface interactions, leading to viscoelastic and frictional heating at the skin and skin/core interface. The horn can be moved along the x-direction (Fig. 1) using different speeds to achieve a continuous weld line of 270 mm. This enabled a relative displacement between the fixed skin/core specimen and the horn during welding. A steel compaction roller of diameter 25 mm and width 40 mm was placed behind the horn at a distance of 70 mm (see Fig. 1), moving at the same speed as the horn along the x-axis to promote effective molecular interdiffusion before the matrix solidification. A constant compaction force of 66 N, corresponding to 1.65 N/mm along the roller length, was maintained throughout the study. Meanwhile, the horn pressure varied across three levels, such as 0.17 MPa, 0.28 MPa, and 0.39 MPa, to evaluate its effect on the skin/core interface under a constant welding speed (5 mm/s). Likewise, three different welding speeds (4 mm/s, 5 mm/s, and 6 mm/s)

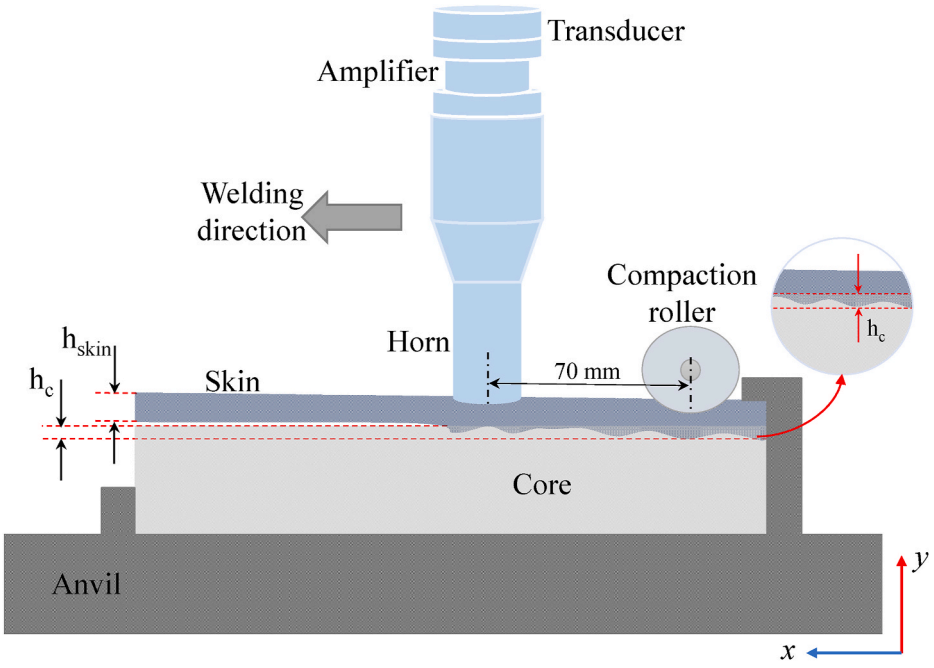

Fig. 1. Diagram illustrating the skin/core welding setup utilising ultrasonic vibration.

were used to examine their impact on the skin/core adhesion under constant horn pressure (0.28 MPa). A steady-state transition into continuous welding was achieved using an electronic motor driver (ABB, Switzerland) while maintaining an appropriate initial holding time to ensure adequate heat transfer across the horn diameter. The PP/glass fibre skin and foam core were positioned on a custom-made anvil during the welding, preventing longitudinal and transverse movement. Both sides of the foam core were bonded to the skin using USW to secure the base of the sandwich structure for Mode I interfacial characterisation. Upon the combined effect of various heat and pressure conditions, a structural collapse, hereafter named as compaction thickness (h_c, in Fig. 1), of the foam core was noticed on both faces, with the extent of the collapse varying under different conditions. To ensure repeatability, five sandwich structures per condition were manufactured for each condition under ambient laboratory conditions (~25 °C, 50 % relative humidity) without pre-drying. The specimens for the Mode I fracture toughness test were cut using a handsaw from the welded sandwich panels, excluding the initial and final sections of the welded panels, as these regions experienced significant core collapsing during welding.

2.3. Mode I fracture toughness

Several non-standardised Mode I testing configurations for sandwich structures are available in the literature. Nonetheless, only a few studies have been carried out utilising the SCB with the roller base set-up [4,25,26]. The Mode I interfacial fracture toughness of sandwich structures was calculated by providing a pure moment at the crack tip of an SCB specimen fixed on a roller base support, as shown in Fig. 2. The hinge was mechanically fastened using screws to the upper skin of the SCB specimen and connected to a Lloyd LR5K universal testing machine equipped with a 5 kN S-type load cell. The hinge transmits a normal load (P) to the partially debonded upper skin, peeling the skin from the core. This artificial pre-crack or initial debond (a_0) was provided using a sharp cutting-edge knife, gently inserted at the skin/core interface to initiate a separation that propagated strictly along or near the interface. A consistent a_0 length was maintained for all specimens to ensure repeatability. Meanwhile, the lower skin was constrained to an aluminium base plate and mounted on a linear hydrostatic roller-bearing carriage. As a result, the top skin behaves like a single cantilever beam supported on an elastic base during loading. The horizontal (shear) components at the crack tips were eliminated through

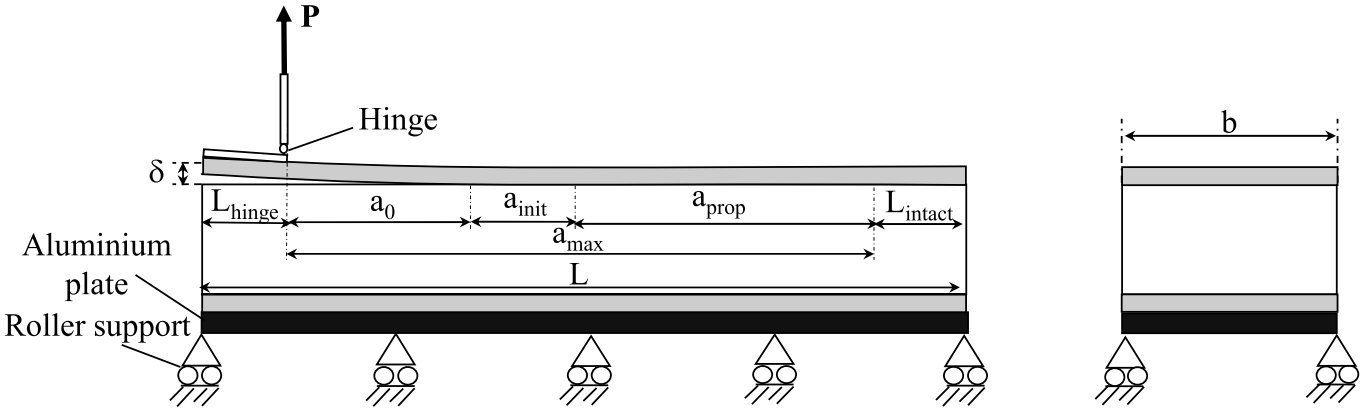

Fig. 2. Schematic representation of the Mode I testing configuration: an SCB resting on a roller base setup.

horizontal roller carriage movements, ensuring dominant Mode I conditions at the crack tips. This guaranteed the application of opening load conditions at the crack tips, avoiding the possibilities of asymmetric loading.

The quasi-static Mode I fracture toughness test was conducted in two phases: a natural crack initiation (a_{init}) phase followed by a crack propagation (a_{prop}) phase. A natural crack of a few millimetres (*i.e.,* a_{init} = 10 mm) was initiated during the first phase at a 2 mm/min loading rate. Subsequently, the crack propagation cycle (a_{prop} = 100 mm) was carried out at a 5 mm/min rate. The load (P) and corresponding load-point displacement (δ) were monitored and recorded during this phase for every 5 mm of crack growth using a high-resolution digital camera (IPEVO VZ-R, China). An average of five samples per condition was considered for computing the Mode I skin/core fracture toughness during the a_{prop} phase. The SCB specimen dimensions were as follows: initial debond length (a_0) = 30 mm, specimen intact length (L_{intact}) = 60 mm, hinge length (L_{hinge}) = 10 mm, length (L) = 210 mm, and width (b) = 20 mm.

Skin thickness variations alter the SCB structure and notably impact the measured interfacial fracture toughness. Unlike the Mode I testing of sandwich structures, as the one adopted in this study, the in-service sandwich structures often featured relatively thin-compliant skins characterised by geometric non-linearity. Consequently, the data reduction method used to measure Mode I fracture toughness in sandwich structures did not adequately account for the in-service specimens. Therefore, it was noted that the obtained results of the Mode I characterisations must be used for comparison among different specimens. Two data reduction schemes were developed to assess Mode I fracture toughness in thin-compliant skin specimens showing non-linear loading behaviour, incorporating specific assumptions to analyse various parametric effects. The first scheme uses linear elastic fracture mechanics (LEFM) through modified beam theory (MBT), while the second disregards LEFM by applying the climbing drum peel (CDP) expression [27].

The expression for calculating the Mode I fracture toughness in sandwich structures was analogous to that used in monolithic fibre-reinforced polymer composites (ASTM 5528M − 21 [28]), and was computed using the principle of LEFM as:

$$G_{Ic_p} = \frac{P^2}{2b}\frac{dC}{da} \tag{1}$$

Here, the specimen compliance, *C*, was determined at each stage of debond growth using the relation δ/*P*. However, this expression for $C = \delta/P$ is only valid for specimens that showed a linearly elastic behaviour, while in our case, this assumption could not hold during crack propagation. The derivative, *dC/da*, was measured from the *C* versus debond (or crack) length (a) relation. By neglecting the non-linearity, the MBT assumed a simplified straight-line relationship for the SCB specimen compliance (C_{SCB}), expressed as:

$$C_{SCB} = m\,(a+\Delta)^3 \tag{2}$$

where *m* was the proportionality constant or slope, indicating the bending rigidity of the SCB specimen. The correction factor, Δ, extended the crack length, allowing the C_{SCB} solution to adjust with the non-zero slope boundary condition. The values for *m* and Δ were obtained from the slope and *x*-intercept of the plot of the cube root of C versus crack length (a). Deriving Eq. (2) for *dC/da* and substituting it into Eq. (1) provided the expression for calculating the Mode I skin/core fracture toughness (G_{Ic_p}) as:

$$G_{Ic_p} = \frac{3P\delta}{2b(a+\Delta)}\ \mathrm{J}\Big/\mathrm{m}^2 \tag{3}$$

Here, the value for *P* and the corresponding *δ* were measured at the onset of each crack growth. Additionally, the G_{Ic_p} was determined for each crack length, where specimen compliance was measured, thereby defining the relationship between fracture toughness (G_{Ic_p}) and crack length (resistance curve or R-curve). The skin/core debonding toughness of the SCB was evaluated as the average of G_{Ic_p} measured for different crack lengths.

The second data reduction method, without incorporating LEFM, was evaluated using a modified climbing drum peel (CDP) expression. This approach was specifically designed for film adhesion and here extended to thin-compliant skin sandwich specimens exhibiting non-linear sawtooth loading behaviour, where the skin stiffness was assumed negligible as in the CDP test. The formula for measuring the skin/core fracture toughness (G_{Ic_p}) based on the CDP test was given in the form [6,24]:

$$G_{Ic_p} = \frac{(P_2 - P_1)\,d}{b\,D}\ \mathrm{J}\Big/\mathrm{m}^2 \tag{4}$$

In the CDP test, P_2 was the load needed to roll up the drum plus the additional load necessary to peel the skin from the core, whereas P_1 accounted for the load to overcome the drum rolling up the skin when no debonding happened. *D* is the total crack length or peeled skin length; *b* is the specimen width; and *d* is the load frame displacement. To consider the skin/core fracture toughness using Eq. (4) in conjunction with the SCB on a roller setup, P_1 was considered to be zero due to the absence of a drum, and P_2 was regarded to be the total (or average) load required to completely peel the skin from the start to end during crack propagation (a_{prop}). The effect of excessive skin bending, which may lead to multiple micro-cracks, was neglected when assessing the load P_2.

2.4. Void content

The effect of welding speeds on void formations in skins during ultrasonic continuous welding was estimated using the immersion method based on Archimedes' principle. Three horn speeds (6 mm/s, 5 mm/s, and 4 mm/s) were used under a constant pressure of 0.28 MPa, and a Kapton film (thickness: 150 μm) was kept at the skin/core interface to prevent skin/core bonding and to allow easy separation of the skin. To avoid edge effects caused by the transient heating conditions at the start and end of the ultrasonic welding process, specimens for density measurement were extracted from the central region of the welded panels. The initial and end portions of the weld were discarded to ensure representative and uniform material properties. A minimum of five 20 × 10 × 1.2 mm^3 coupons from each condition were considered for void measurements. The experimental density (ρ_{ex}) of each skin laminate welded at various speeds was determined under ASTM D 792 [29], using distilled water at 20 °C as the immersion medium. A Radwag density determination kit was used on a Radwag balance with 10^{-4} g accuracy. Moreover, the theoretical density (ρ_{th}) of the same laminates was evaluated utilising the rule of mixtures, based on the resin weight percentage obtained from ASTM D 2584 [30]. The constituent material densities were obtained from manufacturer datasheets, with the glass fibre density assumed as 2540 kg/m^3 and the PP matrix density as 900 kg/m^3. Once the ρ_{ex} and ρ_{th} were measured, an evaluation of the void content (void volume fraction) was followed by the expression:

$$\text{Void content}\ (\%) = \frac{\rho_{th} - \rho_{ex}}{\rho_{th}} \times 100 \tag{5}$$

3. Results and discussion

3.1. Impacts of various welding speeds on fracture toughness

This section aims to identify optimal welding speed (and in Section 3.2, horn pressure) for achieving reliable and defect-free skin/core adhesion or welding in thermoplastic sandwich panels. Optimisation is essentially performed using interfacial fracture toughness, while the obtained results have been interpreted considering the effect of void content, fracture surface morphology, possible skin delamination and collapse of foam cells. Among these, the presence of cohesive failure

within the foam is taken as the primary metric for bond quality, as it reflects superior adhesion at the skin/core interface.

Fig. 3a–d represent the average fracture toughness, load versus displacement curves, $C^{1/3}$ versus crack length, a, and the R-curve for different welding speeds at a constant horn pressure (0.28 MPa). As indicated in Fig. 3b, the load-displacement curves exhibited non-linear loading behaviour, indicating a deviation from the ideal linear elastic conditions assumed in MBT. However, the $C^{1/3}$ versus a plots in Fig. 3c still showed reasonable linear correlations, with coefficient of determination (R^2) values of 0.87, 0.88 and 0.68 and corresponding root mean square error (RMSE) values of 0.034, 0.037 and 0.068 for 4 mm/s, 5 mm/s and 6 mm/s, respectively. Furthermore, the 95 % confidence intervals (CI) for the slope (m), calculated using standard regression methods, demonstrate acceptable consistency, as shown in the inset of Fig. 3c. Given these results, MBT were employed, with a linear loading assumption, to estimate the Mode I fracture toughness. The skin/core fracture toughness determined using both the data reduction schemes, MBT, and the CDP expression, exhibited similar trends with varying speeds, as indicated in Fig. 3a. However, the skin/core fracture toughness values derived from the CDP expression were significantly higher than those determined using MBT. The specimen compliance, C, in MBT, which directly relied on the specimen's stiffness, affected the Mode I fracture toughness measurements. Specifically, MBT tends to underestimate the skin/core Mode I debonding toughness due to the effects of lower specimen stiffness, particularly for specimens with a ductile interface. For instance, in MBT, a reduction of 44 % – 47 % in the average fracture toughness was noted when compared to the values measured using CDP for sandwich specimens with thin-compliant skin. In contrast, the CDP expression, which was relatively C-independent, yielded consistently higher fracture toughness values. The "true" value of G_{Icp} is very likely to be in the interval of the values obtained with MBT and CDP methods, since CDP consistently yielded higher G_{Icp} values than MBT.

Hereon (and similarly in Section 3.2 for horn pressure), the results are discussed based on the data reduced using the MBT. Although MBT assumes linear elastic behaviour, it is widely adopted in the literature for benchmarking interfacial fracture toughness in sandwich structures and allows for direct comparison with previous MBT-based studies. Moreover, the evolution of fracture toughness along the crack length (R-curve) can only be evaluated using MBT, as the CDP method provides a single, averaged value of fracture toughness and does not account for crack growth behaviour. Therefore, in this study, MBT is employed as a conservative estimation tool, not as a substitute for a compliance-independent CDP approach, but to facilitate trend comparison and R-curve analysis. The limitations of MBT under nonlinear conditions are acknowledged, and complementary analysis, *i.e.*, CDP, is provided to support the interpretation.

The morphology of the fractured skin/core surfaces, along with corresponding schematic illustrations (shown on the right), is reported in Fig. 4a–c, illustrating the skin/core bonding behaviour across various

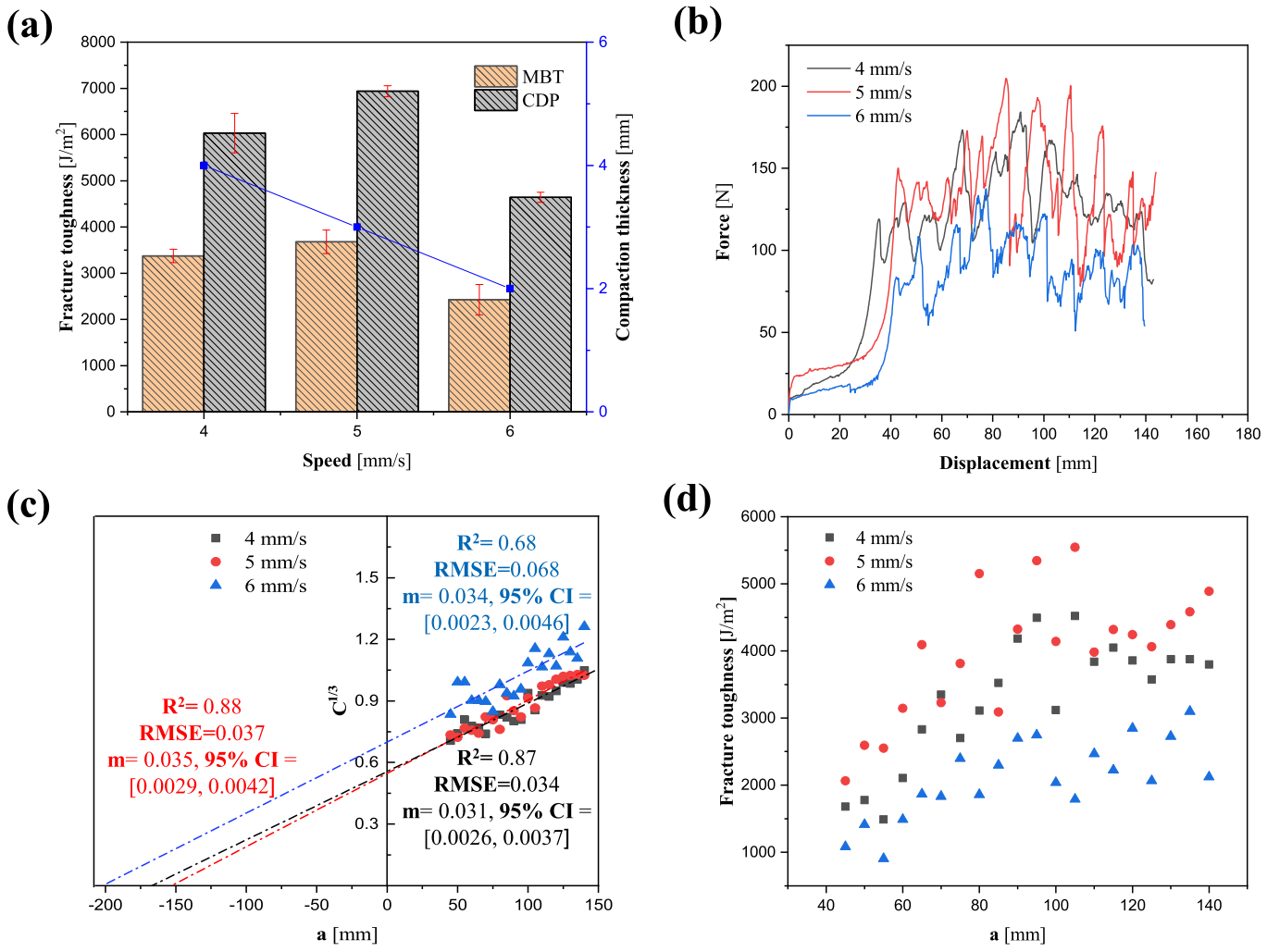

Fig. 3. a) Average fracture toughness, b) Load versus displacement plots, c) $C^{1/3}$ versus a, and d) R-curve of the specimens welded under 4 mm/s, 5 mm/s, and 6 mm/s at 0.28 MPa.

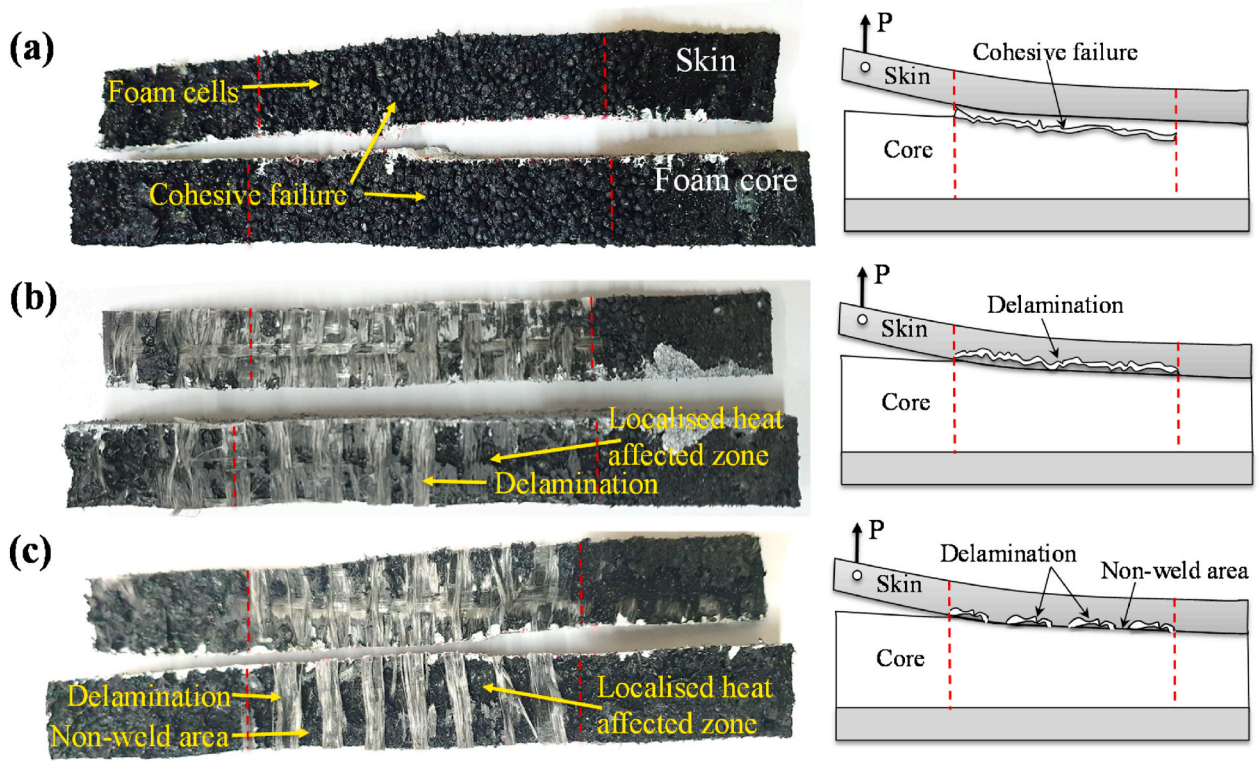

Fig. 4. Fractured skin/core surface images and corresponding schematic side view representations of failure modes at welding speeds a) 4 mm/s, b) 5 mm/s, and c) 6 mm/s. The red dashed line marks the region of crack propagation during Mode I SCB testing. (For interpretation of the references to colour in this figure legend, the reader is referred to the Web version of this article.)

welding speeds (4 mm/s, 5 mm/s, and 6 mm/s). The longer horn contact duration at the lower speed of 4 mm/s generated a more uniform heat distribution at the skin/core interface. As a result, more uniform melting occurred at the skin/core interface, facilitating better interdiffusion of molecular chains of the skin and core matrix. The difference in modulus at the skin/core interface induced positive shear, causing the crack to kink into the soft foam core and resulting in cohesive failure. Cohesive failure was evident from the adhesion of foam cells to the fractured skin surface, indicating strong interfacial bonding, as depicted in Fig. 4a. Correspondingly, the skin/core welding at a lower speed of 4 mm/s resulted in a 39 % higher fracture toughness than the specimen welded at a higher speed of 6 mm/s (see Fig. 3a); however, this value is only useful for trend comparison, as both specimens exhibited the same failure mode. Similar findings, when lower welding speeds are used, were noted in the studies involving glass fibre-reinforced polyetheretherketone (PEEK) skins and a 3D-printed polyetherimide (PEI) honeycomb core, using induction welding under vacuum [8,31]. Likewise, the USW of FRTPCs at lower speeds reported comparable effects of welding speed [20,32]. Therefore, the improved bonding at 4 mm/s is primarily attributed to the cohesive failure mode and supported by the fracture toughness trend.

Skin/core specimens welded at the highest welding speed (6 mm/s) showed the lowest value of fracture toughness, attributed to the reduced contact time during welding. Therefore, a higher welding speed leads to less uniform temperature distribution at the skin/core interface. This results in several non-welded or unmelted areas and localised heat-affected zones, as observed on the fractured skin/core surfaces in Fig. 4c. This leads to a weak skin/core adhesion, resulting in lower load-displacement and resistance curve characteristics, as shown in Fig. 3b and d. A similar observation of numerous unmelted areas was reported by Senders et al. [32] during high-speed USW of carbon fibre/PPS laminates, resulting in reduced weld joint strength. At welding speeds of 5 and 6 mm/s, the crack kinked into the skin (negative shear) during the Mode I test, producing a localised delamination (Fig. 4b and c). The skin was partially delaminated, suggesting that some skin interlaminar damage could occur. Oliveira et al. [15] detailed comparable localised delamination around certain connections during bending tests on ultrasonically welded HDPE-based GFRP skins and a honeycomb core. To determine whether the US heating can produce delamination, the void content in skins was measured as described in Section 2.4. As observed in Fig. 5, the skins welded at the highest speed (6 mm/s) were

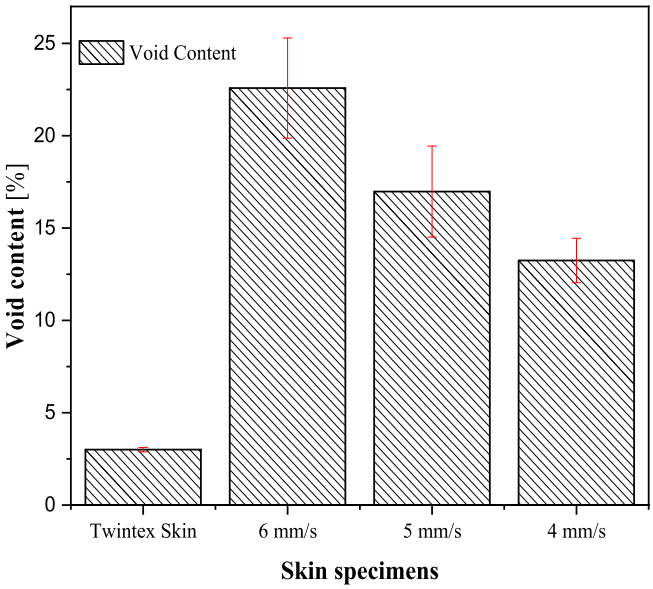

Fig. 5. Apparent void content of the skin at various welding speeds during continuous skin/core USW.

characterised by the highest void content among all welded skin laminates (>20 %), with an apparent void content of 70 % greater than those welded at a lower speed of 4 mm/s. Furthermore, the standard deviation in Fig. 5 was observed to decrease with the decrease in welding speed. This suggests that welding speed significantly influences void formation, with faster speeds leading to increased porosity and a higher risk of delamination within the skin. Notably, the unwelded Twintex® skin demonstrated a much lower void percentage compared to all welded skin laminates, providing a baseline assessment for the impact of the welding process on the quality of skin laminates (see Fig. 5). The actual void content in the skins of the sandwich structure may differ slightly from the measured one due to the diffusion of the foam polymer, which can fill up the voids formed in the skin during welding.

A relatively longer horn contact time at a welding speed of 5 mm/s promoted more uniform heating at the skin/core weld interface compared to what was observed at 6 mm/s. This enhanced skin/core bonding while minimising defects such as localised heat-affected zones and non-weld areas, as shown in Fig. 4b. Also, a reduced skin delamination was observed, attributed to a lower skin void formation, on the fractured surfaces of skin/core specimens welded at 5 mm/s (Fig. 4b) compared to those welded at 6 mm/s (Fig. 4c). When crack propagation occurred through the stiff skin, as in specimens welded at 5 mm/s, the measured fracture toughness was 51 % and 10 % higher than those welded at 6 mm/s and 4 mm/s, respectively (Fig. 3a). Although fracture toughness appears higher at the skin/core welded at 5 mm/s, the failure occurred in the skin, and thus the value reflects the skin's toughness, not the skin/core interfacial bond. Therefore, this value should not be interpreted as an indicator of improved interface strength. In line with the evaluation criteria of this study, cohesive failure in the foam core, as observed at 4 mm/s, remains the primary measure of bond quality. Thus, although 5 mm/s exhibited improved processing uniformity and reduced voids, it led to a weakening of interlaminar adhesion of the skin that promoted crack propagation in the skin.

The heat generation and distribution of temperature at different welding speeds significantly influenced the compaction thickness (h_c) or the collapsing of the foam core. Therefore, the compaction thickness increases with the decrease in welding speed, as represented in Fig. 3a. At higher speeds (e.g., 6 mm/s), a less uniform heat generation leads to lower softening and deformation of foam, resulting in reduced compaction thickness (2.0 ± 0.5 mm) due to incomplete melting or bonding and localized heating. On the other hand, lower speeds (e.g., 4 mm/s) provided uniform heat distribution, promoting better foam softening, molecular interdiffusion, and increased compaction thickness to 4.0 ± 0.3 mm. Moderate speeds (e.g., 5 mm/s) under 0.28 MPa achieved a balance, resulting in controlled foam compaction of 3.0 ± 0.2 mm with fewer defects compared to higher speeds (6 mm/s). However, despite its balanced compaction, the interfacial bonding at 5 mm/s was not measured since the failure occurred in the skin rather than in the foam, due to a weakening of interlaminar adhesion in the skin when this process condition is used. The higher compaction at 4 mm/s, on the other hand, supported deeper polymer interdiffusion and resulted in cohesive failure within the foam, indicating stronger skin/core adhesion. At the same time, the effects of temperature increase under the horn and pressure applied by the roller did not promote a weakening in the interlaminar adhesion of the skin. This highlights that while compaction thickness can serve as a useful indicator of thermal efficiency and interdiffusion potential, it must be interpreted along with the failure mode to assess adhesion quality accurately. Therefore, a slight variation in speed could drastically vary the interface temperature, affecting the quality of the skin/core bonding.

3.2. Effect of different horn pressures on fracture toughness

In this study, welding speed was fixed at 5 mm/s, which was selected based on a relatively suboptimal bonding characteristics observed at higher welding speeds, with balanced compaction thickness and minimal defects in preliminary tests. Although a lower welding speed of 4 mm/s at 0.28 MPa produced stronger bonding (cohesive failure), it also resulted in higher foam compaction compared to 5 mm/s. In contrast, the 5 mm/s condition, while exhibiting more balanced compaction, showed evidence of skin delamination and partial non-welded regions. Therefore, 5 mm/s was chosen as an experimental baseline for assessing the influence of horn pressure across a wide range, to improve interfacial bonding and reduce defects through pressure optimisation. Hence, the welding behaviour using various horn pressures (0.17 MPa, 0.28 MPa, and 0.39 MPa) under a constant welding speed of 5 mm/s was analysed according to MBT and CDP Mode I fracture toughness data reduction, as shown in Fig. 6a–d. This includes fracture toughness, load versus displacement plots, cube root of specimen compliance versus crack length, and R-curves. Fig. 7a–c presents the morphologies of the corresponding skin/core fractured surfaces (shown on the left), and the schematic side view illustrating the failure modes is reported on the right.

The SCB results demonstrated the transition in failure modes at the interface and reflected the kinetics of heat generation and distribution during continuous skin/core welding. In comparison, specimens welded under high horn pressure (0.39 MPa) provide 44 % higher average fracture toughness than low horn pressure of 0.17 MPa, as summarised in Fig. 6a. A higher horn pressure (0.39 MPa) favours consistent surface contact between the two adherents and uniform heat dissipation by friction at the horn/skin interface and skin/foam interface. Therefore, during the Mode I loading, the mismatch in material moduli at the interface promotes crack propagation through the soft foam core, leading to cohesive failure, as shown in Fig. 7c. Furthermore, as reported in Section 3.1, the skin/core specimens welded at a speed of 5 mm/s under all horn pressures showed skin delamination due to a weakening of interlaminar adhesion during welding, as illustrated in Fig. 7a–c. However, specimens welded at a horn pressure of 0.39 MPa demonstrated relatively lower skin delamination at the interface (see Fig. 7c). Skin heating above the matrix melting temperature was responsible for delamination, while higher horn pressure limited this phenomenon by improving contact and enhancing molecular diffusion at the interface. The uniform melting induced by high horn pressure at the skin/core interface can facilitate matrix diffusion into the skin, effectively filling voids and limiting the risk of delamination. Additionally, the roller can promote re-consolidation if, during this action, the temperature passes through the crystallisation range. Similar findings were reported by Jongbloed et al. [33] during the static welding performed in carbon fibre/PPS laminates, in which higher consolidation (horn) pressures minimise the defects at the weld line and ensure better weld quality. A similar effect was observed with the hybrid welding of CFRP/Al joints [14]. Conversely, at lower pressure, the exerted horn pressure of 0.17 MPa was likely inadequate to eliminate the initial air gaps within the horn and the skin, as well as at the weld interface. Consequently, inconsistent surface contacts lead to non-uniform heating and energy transfer during continuous USW, causing several non-weld areas and localised heat-affected zones at the interface, as shown in Fig. 7a. This change in heating influences interface failure modes and can lead to localised skin delamination (see Fig. 7a) and a subsequent reduction in fracture toughness, load-displacement, and R-curve characteristics, as illustrated in Fig. 6a, b, and 6d. At a horn pressure of 0.28 MPa, the crack propagated through the weakened stiff skin (see Fig. 7b), resulting in delamination. The increased fracture toughness compared to the one measured at 0.17 MPa and 0.39 MPa was influenced by the fracture energy associated with skin delamination (Fig. 6a). Therefore, the measured Mode I fracture toughness at this condition reflects the fracture resistance of the skin itself and should not be interpreted as a sign of enhanced skin/core interfacial bonding.

Variations in heat generation and its distribution under different horn pressures significantly affect the compaction of the foam cells at the interface. As shown in Fig. 6a, the foam cell collapse or h_c increases with higher horn pressure. Higher horn pressure (0.39 MPa) reduces air

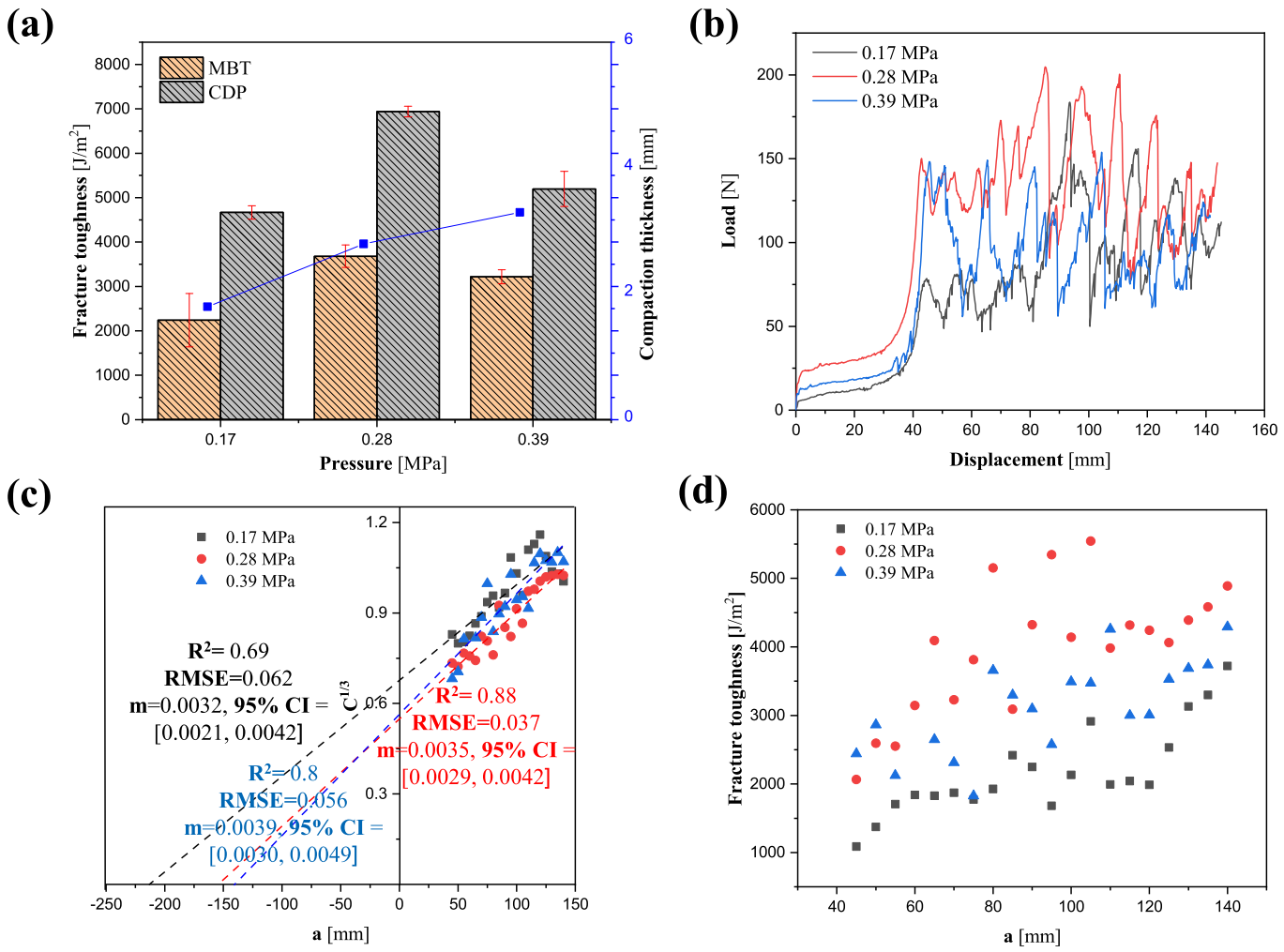

Fig. 6. Effect of horn pressure on a) Average fracture toughness, b) Load versus displacement curves, c) $C^{1/3}$ versus *a*, and d) R-curve of the specimens welded at 5 mm/s.

gaps and ensures uniform heating and melting across the entire weld interface, exhibiting 75 % higher collapse of foam than specimens welded at 0.17 MPa. As previously noted, a balanced and controlled foam cell collapse or compaction thickness (h_c) was observed with 0.28 MPa under 5 mm/s welding speed, representing an intermediate response between the higher collapse at 0.39 MPa and the lower collapse at 0.17 MPa. Nonetheless, as with welding speed, compaction thickness alone is not enough to assess interfacial bonding. The observed failure modes must also be considered to determine whether the compaction led to improved bonding or structural degradation.

4. Conclusions

To address the manufacturing challenges of thermoplastic sandwich structures, a continuous skin/core ultrasonic welding system was designed by incorporating a horn and a compaction roller moving simultaneously along the skin/core interface. The skin/core weld quality of the sandwich panel was characterised and optimised using different speeds and horn pressures through the SCB Mode I test. Two modified data reduction schemes, based on the MBT and CDP expressions, were implemented with specific assumptions to measure fracture toughness.

Modified data reduction methods show comparable trends in average fracture toughness across different welding parameters. However, the compliance-independent CDP expression measures higher fracture toughness values than the compliance-dependent MBT method. Fracture toughness measurements utilising both data reduction methods can be adopted for parametric comparison and optimisation purposes. Challenges in measuring fracture toughness using the compliance-dependent MBT, as well as conformity variations with drum diameters in the CDP test, compromise measurement accuracy. These issues can be addressed by employing the modified CDP expression with the SCB test with roller base support, ensuring reliable parametric comparison and optimisation for compliant skin sandwich panels.

It also highlighted the effect of US heat generation on skin delamination, which, in turn, conversely affects the value of interfacial fracture toughness. As a consequence, under certain processing conditions (low-to-medium pressure, medium-to-high speed), the SCB test promotes crack propagation between skin plies (*i.e.,* delamination occurs), yielding results that differ but are not representative of the skin/core adhesion. These outcomes demonstrate that fracture toughness alone cannot reliably indicate bond quality when failure modes differ. Strong interfacial bonding was achieved at 4 mm/s under 0.28 MPa and at 5 mm/s under 0.39 MPa, both exhibiting cohesive failure. Although welding speed and horn pressure were studied independently, results demonstrate their interdependent effect on bonding. Lastly, some foam core collapse at the weld interface was always present, leading to a reduction in total sandwich thickness.

CRediT authorship contribution statement

Amal Alliyankal Vijayakumar: Writing – original draft,

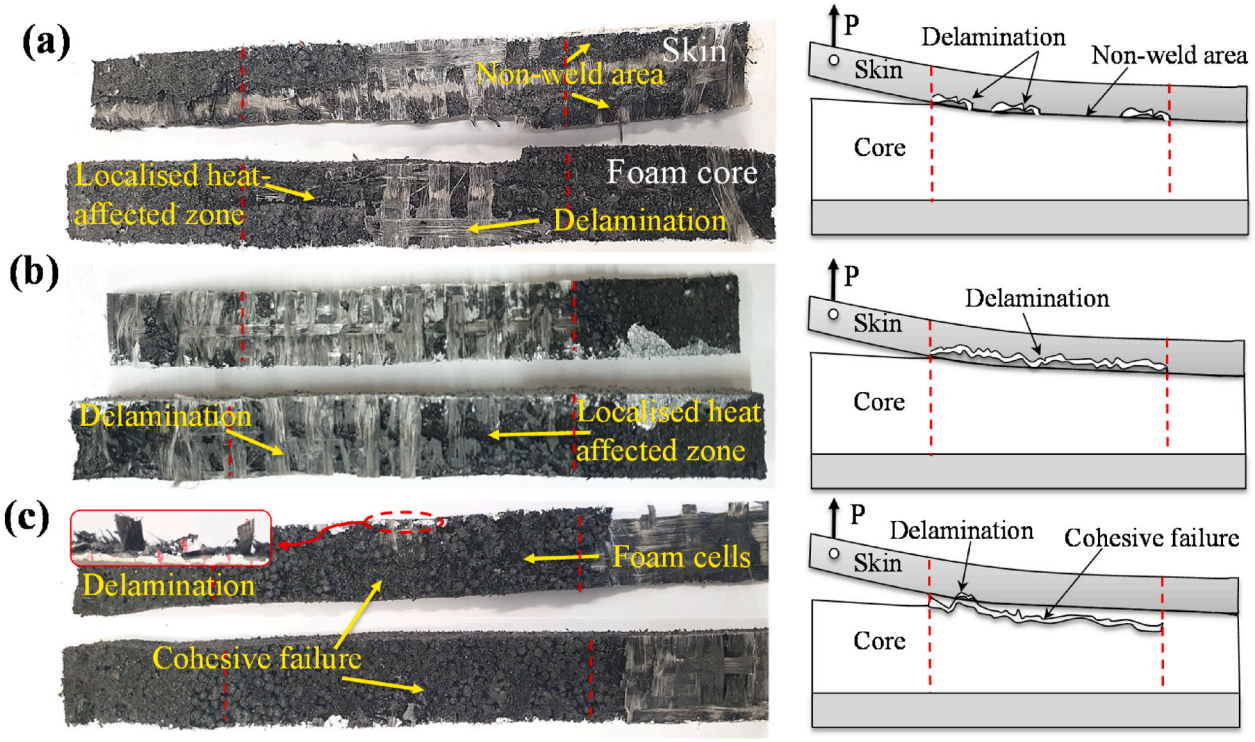

Fig. 7. Observed fractured skin/core surfaces and schematic side view illustrations of damage modes welded at different pressures: a) 0.17 MPa, b) 0.28 MPa, and c) 0.39 MPa. The red dashed line indicates the region of crack propagation during testing. (For interpretation of the references to colour in this figure legend, the reader is referred to the Web version of this article.)

Visualization, Validation, Methodology, Investigation, Formal analysis, Data curation, Conceptualization. **Muhammad Zahid:** Writing – review & editing, Supervision, Project administration, Funding acquisition, Formal analysis. **Stefano G. Corvaglia:** Writing – review & editing, Supervision, Project administration, Funding acquisition. **Francesco Montagna:** Visualization, Resources. **Francesca Lionetto:** Writing – review & editing, Validation, Supervision, Resources, Project administration, Formal analysis. **Alfonso Maffezzoli:** Writing – review & editing, Supervision, Resources, Project administration, Methodology, Formal analysis, Conceptualization.

Declaration of competing interest

The authors declare the following financial interests/personal relationships, which may be considered as potential competing interests. Amal Alliyankal Vijayakumar reports that financial support was provided by Leonardo S.p.A. If there are other authors, they declare that they have no known competing financial interests or personal relationships that could have appeared to influence the work reported in this paper.

Acknowledgement

The author(s) acknowledge financial support of the PhD scholarship of Amal Alliyankal Vijayakumar from Leonardo S.p.A., Italy.

Data availability

Data will be made available on request.

References

[1] Gao X, Zhang M, Huang Y, Sang L, Hou W. Experimental and numerical investigation of thermoplastic honeycomb sandwich structures under bending loading. Thin-Walled Struct 2020;155:106961. https://doi.org/10.1016/j.tws.2020.106961.
[2] Grünewald J, Parlevliet P, Altstädt V. Manufacturing of thermoplastic composite sandwich structures: a review of literature. J Thermoplast Compos Mater 2017;30:437–64. https://doi.org/10.1177/0892705715604681.
[3] Passaro A, Corvaglia P, Manni O, Barone L, Maffezzoli A. Processing-properties relationship of sandwich panels with polypropylene-core and polypropylene-matrix composite skins. Polym Compos 2004;25:307–18. https://doi.org/10.1002/pc.20025.
[4] Irven G, Duncan A, Whitehouse A, Carolan D, Fergusson A, Dear JP. Impact response of composite sandwich structures with toughened matrices. Mater Des 2021;203:109629. https://doi.org/10.1016/j.matdes.2021.109629.
[5] Carlsson LA, Kardomateas GA. Structural and failure mechanics of sandwich composites, vol 121. Dordrecht: Springer Netherlands; 2011. https://doi.org/10.1007/978-1-4020-3225-7.
[6] Weidmann F, Ziegmann G, Wieser J. A review of mode I dominant interfacial fracture toughness test methods of skin-core bonding for thermoplastic composite sandwich structures. J Thermoplast Compos Mater 2023;36:2643–73. https://doi.org/10.1177/08927057221083493.
[7] Wilk J. Investigation of the applicability of single cantilever beam test for the evaluation of fracture toughness of sandwich composites. Eng Fract Mech 2023;281:109075. https://doi.org/10.1016/j.engfracmech.2023.109075.
[8] Martin RG, Johansson C, Tavares JR, Dubé M. Manufacturing of thermoplastic composite sandwich panels using induction welding under vacuum. Compos Appl Sci Manuf 2024;182:108211. https://doi.org/10.1016/j.compositesa.2024.108211.
[9] Denkena B, Schmidt C, Schmitt C, Kaczemirzk M. Experimental investigation on the use of a PEI foam as core material for the In-Situ production of thermoplastic sandwich structures using laser-based thermoplastic automated fiber placement. Materials 2022;15:7141. https://doi.org/10.3390/ma15207141.
[10] Gutnik VG, Gorbach NV, Dashkov AV. Some characteristics of ultrasonic welding of polymers. Fibre Chem 2002;34:426–32. https://doi.org/10.1023/A:1022912325343.
[11] Zhao T, Broek C, Palardy G, Villegas IF, Benedictus R. Towards robust sequential ultrasonic spot welding of thermoplastic composites: welding process control strategy for consistent weld quality. Compos Appl Sci Manuf 2018;109:355–67. https://doi.org/10.1016/j.compositesa.2018.03.024.
[12] Zhao T, Zhao Q, Wu W, Xi L, Li Y, Wan Z, et al. Enhancing weld attributes in ultrasonic spot welding of carbon fibre-reinforced thermoplastic composites: effect of sonotrode configurations and process control. Compos B Eng 2021;211:108648. https://doi.org/10.1016/j.compositesb.2021.108648.
[13] Lionetto F, Balle F, Maffezzoli A. Hybrid ultrasonic spot welding of aluminum to carbon fiber reinforced epoxy composites. J Mater Process Technol 2017;247:289–95. https://doi.org/10.1016/j.jmatprotec.2017.05.002.

[14] Lionetto F, Mele C, Leo P, D'Ostuni S, Balle F, Maffezzoli A. Ultrasonic spot welding of carbon fiber reinforced epoxy composites to aluminum: mechanical and electrochemical characterization. Compos B Eng 2018;144:134–42. https://doi.org/10.1016/j.compositesb.2018.02.026.
[15] Oliveira PR, Virgen GPG, Imbert M, Beisel S, May M, Panzera TH, et al. Ultrasonically welded eco-friendly sandwich panels based on upcycled thermoplastic core: an eco-mechanical characterisation. Resour Conserv Recycling Adv 2023;20:200187. https://doi.org/10.1016/j.rcradv.2023.200187.
[16] Xiang J, Tao J, Yang F, Li H, Chen X, Lin Y, et al. Joint interface optimization of all-CFRTP composite honeycomb prepared by ultrasonic multi-spot welding. Compos Sci Technol 2024;248:110456. https://doi.org/10.1016/j.compscitech.2024.110456.
[17] Wang Y, Rao Z, Liao S, Wang F. Ultrasonic welding of fiber reinforced thermoplastic composites: current understanding and challenges. Compos Appl Sci Manuf 2021;149:106578. https://doi.org/10.1016/j.compositesa.2021.106578.
[18] Unnikrishnan TG, Kavan P. A review study in ultrasonic-welding of similar and dissimilar thermoplastic polymers and its composites. Mater Today Proc 2022;56:3294–300. https://doi.org/10.1016/j.matpr.2021.09.540.
[19] Lionetto F, Dell'Anna R, Montagna F, Maffezzoli A. Modeling of continuous ultrasonic impregnation and consolidation of thermoplastic matrix composites. Compos Appl Sci Manuf 2016;82:119–29. https://doi.org/10.1016/j.compositesa.2015.12.004.
[20] Köhler F, Fernandez Villegas I, Dransfeld C, Herrmann A. On the influence of welding parameters and their interdependence during robotic continuous ultrasonic welding of carbon fibre reinforced thermoplastics. Materials 2024;17:5282. https://doi.org/10.3390/ma17215282.
[21] Villegas IF. In situ monitoring of ultrasonic welding of thermoplastic composites through power and displacement data. J Thermoplast Compos Mater 2015;28:66–85. https://doi.org/10.1177/0892705712475015.
[22] Vijayakumar AA, Zahid M, Corvaglia SG, Maffezzoli A. Skin/core fracture toughness of sandwich structures: a comparison of different experimental arrangements. Polym Test 2025;150:108904. https://doi.org/10.1016/j.polymertesting.2025.108904.
[23] Li X, Carlsson LA. The Tilted Sandwich Debond (TSD) specimen for Face/Core interface fracture characterization. Jnl Sandwich Struct Mater 1999;1:60–75. https://doi.org/10.1177/109963629900100104.
[24] Nettles AT, Gregory ED, Jackson JR. Using the Climbing Drum Peel (CDP) test to obtain a GIC value for Core/Face sheet bonds. J Compos Mater 2007;41:2863–76. https://doi.org/10.1177/0021998307079974.
[25] Cantwell WJ, Davies P. A test technique for assessing core-skin adhesion in composite sandwich structures. J Mater Sci Lett 1994;13:203–5. https://doi.org/10.1007/BF00278162.
[26] Cantwell WJ, Davies P. A study of skin-core adhesion in glass fibre reinforced sandwich materials. Appl Compos Mater 1996;3:407–20. https://doi.org/10.1007/BF00133683.
[27] Trucillo P, Vijayakumar AA, Zahid M, Maffezzoli A, Di Maio E. Manufacturing of PP-Based composite sandwich panels via simultaneous foaming and skin-core bonding. Polym Compos 2025;46. https://doi.org/10.1002/pc.70287.
[28] ASTM D5528-21. Standard test method for mode I interlaminar fracture toughness of unidirectional fiber-reinforced polymer matrix composites. West Conshohocken, PA: ASTM International; 2021.
[29] ASTM D792-20. Standard test methods for density and specific gravity (relative density) of plastics by displacement. West Conshohocken, PA: ASTM International; 2020.
[30] ASTM D2584-18. Standard test method for ignition loss of cured reinforced resins. West Conshohocken, PA: ASTM International; 2018.
[31] Martin RG, Johansson C, Tavares JR, Dubé M. CF/PEEK skins assembly by induction welding for thermoplastic composite sandwich panels. Compos B Eng 2024;284:111676. https://doi.org/10.1016/j.compositesb.2024.111676.
[32] Senders F, van Beurden M, Palardy G, Villegas IF. Zero-flow: a novel approach to continuous ultrasonic welding of CF/PPS thermoplastic composite plates. Adv Manuf Polym Compos Sci 2016;2:83–92. https://doi.org/10.1080/20550340.2016.1253968.
[33] Jongbloed B, Vinod R, Teuwen J, Benedictus R, Villegas IF. Improving the quality of continuous ultrasonically welded thermoplastic composite joints by adding a consolidator to the welding setup. Compos Appl Sci Manuf 2022;155:106808. https://doi.org/10.1016/j.compositesa.2022.106808.